Cross sections of proton-induced neutron emission reactions on thorium and uranium at energies below 18 MeV

T. V. Kotanjyan,[1,*] A. Y. Aleksanyan,[1] A. O. Kechechyan,[2] S. M. Amirkhanyan,[1] D. A. Martiryan,[1] H. R. Gulkanyan,[1] and L. A. Poghosyan[1]

[1]*Alikhanyan National Science Laboratory, 0036 Yerevan, Armenia*

[2]*Joint Institute for Nuclear Research (JINR), 141980 Dubna, Russian Federation*

(Received 23 August 2023; revised 19 February 2024; accepted 30 April 2024; published 10 June 2024)

Experimental data on proton-induced neutron emission reactions in actinides are important for nuclear astrophysics, nuclear energy, and medical applications. Presently existing data on (p, xn) reactions in thorium and uranium at low energies range ($E_p < 20$ MeV) are somewhat scarce and often contradict each other. In this work, the cross sections of proton-induced ^{232}Th$(p, n)^{232}$Pa, ^{232}Th$(p, 3n)^{230}$Pa, ^{238}U$(p, n)^{238}$Np, ^{238}U$(p, 3n)^{236m}$Np, and ^{238}U$(p, np)^{237}$U reactions are measured at the proton energy range 12–17 MeV using the stacked-foil technique and with the induced activation method. γ-ray spectroscopy is used to identify the resulting radionuclides and to determine their yields. In total, there are 21 cross sections determined in this work for the listed reactions. This new data set can help to clear up the discrepancies between existing data sets from different experiments, as well as to fill in the gap of missing low-energy data. The cross-section data are compared to the predictions of the nuclear reactions simulation code TALYS1.96, using different combinations of options of several main ingredients of the code, such as the photon strength function, the optical model potential, the fission barrier, the nuclear level density, and the pre-equilibrium mechanism.

DOI: 10.1103/PhysRevC.109.065802

I. INTRODUCTION

Nuclear transformations induced by galactic cosmic rays (GCRs) in the interstellar medium and by solar energetic particles (SEPs) in the circumsolar medium influence the elemental and isotopic composition of stellar and planetary surfaces, meteorites, and cosmic dust (see Ref. [1] and references therein). The main component of the GCRs and the SEPs initiating inelastic nuclear reactions are protons with their overwhelming fraction occupying the energy range below 100 MeV (see, e.g., Ref. [2]). One of the basic ingredients of theoretical models elaborated for the description of the aforementioned transformations are inelastic cross sections of proton-nuclear interactions. These concern proton-induced reactions on actinide nuclei, in particular, (p, xn) reactions on ^{232}Th and ^{238}U. The available experimental data on these reactions is sometimes scarce and the results are often contradictory if available, specifically at incident energies up to a few tens of MeV [3–16]. The aim of this work is to rectify the situation by measuring the following proton-induced reaction cross sections: ^{232}Th$(p, n)^{232}$Pa, ^{232}Th$(p, 3n)^{230}$Pa, ^{238}U$(p, n)^{238}$Np, ^{238}U$(p, 3n)^{236m}$Np, and ^{238}U$(p, np)^{237}$U at several energies below 18 MeV. The new measurement results can help to clarify the discrepancies between existing data sets from different experiments, as well as to fill in the gap for nonexistent cross sections at low energies. An example is the data for the ^{238}U$(p, np)^{237}$U reaction. In addition to being of astrophysical interest, this type of data [for example in the ^{232}Th$(p, 3n)^{230}$Pa reaction] can also have medical applications. Low energy proton-induced reaction cross-section data can support, for example, the targeted α therapy that utilizes the decay series of α-particle-emitting radionuclide ^{230}U to apply a localized, cytotoxic dose of α radiation to tumor cells (see, e.g., Refs. [7,9]). New experimental data can also be useful for testing predictions of reaction models at low energies.

The experiment was carried out at A. Alikhanyan National Science Laboratory (AANL) using the 18-MeV proton beam of the C-18 cyclotron. The proton-induced activation method was utilized in the experiment. The yields were determined by γ-ray spectroscopy of the irradiated thorium and uranium targets. The description of the experimental procedure is given in Sec. II. The experimental results and their comparison to the data from other works and to the theoretical predictions of the TALYS1.96 code are presented in Secs. III and IV, respectively, with a final summary and conclusion in Sec. V.

II. EXPERIMENTAL PROCEDURE

A. Target system and irradiation

The target system consists of nine consecutive assemblies of stacked disk-shaped foils of 12 mm diameter. Each assembly consisted of a 20-μm-thick copper foil followed by a target made from a deposition of a natural uranium or thorium thin layer on Al backing (of 23.5 and 33.5 μm thickness, for thorium and uranium targets, respectively). The masses

*tigran.kotanjyan@mail.yerphi.am

 ©2024 American Physical Society

of uranium and thorium layers were determined by γ-ray spectroscopy analysis using the natural γ activity of the ^{238}U and ^{232}Th decay series, around the $E_\gamma = 1001.0$-keV line of the radioisotope ^{234m}Pa and the $E_\gamma = 238.6$-keV line of the radioisotope ^{212}Pb, respectively. The γ-ray spectroscopy measurements were performed at the AANL underground low-background laboratory located at the Avan salt mine near Yerevan. γ rays were measured with an experimental setup based on a high-purity germanium (HPGe) detector (see below). The ambient background contribution (composed $9\% \pm 1\%$ and $20\% \pm 2\%$ of the aforementioned γ lines of ^{238}U and ^{232}Th decay series, respectively) was subtracted from the measured activity. The masses of all individual layers were estimated. The average masses of uranium and thorium layers were equal to 1.058 ± 0.070 and 1.087 ± 0.068 mg, respectively. The quoted errors were mainly due to systematic errors caused by the uncertainty (about 5%) in the measured efficiency of the HPGe detector.

The target system was inserted into the NIRTA container [17] and exposed in the extracted proton beam of the C-18 cyclotron for 10 min. Copper foils and Al backings serve as proton energy degraders and provide desirable mean energy of protons in each of the thorium and uranium layers. The degradation of proton energy E_p throughout the target stack was calculated using the SRIM code [18] resulting in a variation of the E_p mean value from 17.00 ± 0.36 to 12.00 ± 0.21 MeV for the first and last uranium layers, and from 16.43 ± 0.08 to 12.68 ± 0.18 MeV for the first and last thorium layers. For copper foils this variation was from 17.40 ± 0.05 to 12.51 ± 0.19 MeV. The beam intensity at each target location was determined as shown below.

B. γ-ray spectroscopic measurements

The induced activity of the targets was used to measure the yields of radionuclides. The γ-ray spectroscopic measurements were carried out in the AANL underground laboratory [19,20] located at a depth of 650 m of water equivalent. A HPGe GCD-20180 germanium detector was used in measurements. The diameter, length, and sensitive volume of the germanium crystal were, respectively, 51.7 mm, 49.05 mm, and 101.2 cm^3. The detector resolution at 1.33 MeV was 1.8 keV. The relative registration efficiency at 1.33 MeV is equal to 20%. The detector was surrounded by a shielding of low-activity lead and copper to suppress the influence of the external background. To prevent radon from entering the setup, the detector was wrapped in a polyethylene bag that was purged with nitrogen. A detailed description of the germanium detector and its calibration procedure is presented in detail in Ref. [20].

The copper foils were made of natural copper with 69.1% ^{63}Cu and 30.9% ^{65}Cu isotopes. They were used to measure the yield of the ^{65}Cu$(p, n)^{65}$Zn monitor reaction. The well-known E_p dependence of the monitor reaction cross section $\sigma_m(E_p)$ [21] (recommended by the IAEA) allows one to estimate the mean current I_p^i $(i = 1, \ldots, 9)$ in each copper foil. As a result of γ-ray spectroscopic analysis of irradiated copper foils, the estimated values of I_p for all of them turned out to be comparable within statistical errors, with a value averaged over all foils of $I_p = 0.721 \pm 0.054 \mu$A, where the quoted error included also 4.2% uncertainty in $\sigma_m(E_p)$ [21].

III. MEASUREMENT RESULTS AND DISCUSSION

The following reactions were considered in this work:

$$^{232}\text{Th}\,(p, n)^{232}\text{Pa}, \tag{1}$$

$$^{232}\text{Th}\,(p, 3n)^{230}\text{Pa}, \tag{2}$$

$$^{238}\text{U}\,(p, n)^{238}\text{Np}, \tag{3}$$

$$^{238}\text{U}\,(p, 3n)^{236m}\text{Np}, \tag{4}$$

$$^{238}\text{U}\,(p, np)^{237}\text{U}. \tag{5}$$

In reaction (5) the final (np) system comprises both a deuteron and an unbound neutron-proton pair. All daughter products of reactions (1)–(5) listed above are radionuclides and can be identified by γ rays accompanying their decays. We do not consider here two-neutron emission $(p, 2n)$ reactions, since their daughter nuclei ^{231}Pa and ^{237}Np are α radioactive and their decays are not accompanied by sufficiently intense γ rays.

Table I summarizes the decay parameters (taken from Ref. [22]) used for the identification of daughter radionuclides in reactions (1)–(5) and the measurements of their yields, as well as the γ detection efficiencies. The γ-ray spectroscopic analysis around the 94–98-keV region is complicated due to the contribution of adjacent lines $E_\gamma = 97.1$ keV and $E_\gamma = 101.1$ keV belonging to the daughter nucleus ^{237}U from reaction (5). The yields of the daughter nuclei ^{236m}Np and ^{237}U were, therefore, estimated simultaneously from a combined analysis of γ-ray spectra in a relatively wide interval of $E_\gamma = 93 - 102$ keV. An independent estimation of the ^{237}U yield was also done using its line $E_\gamma = 208.0$ keV.

The reliability of the identification of daughter nuclei was verified by multiple spectroscopic measurements and the decay curve analysis resulting in the following half-life values: $T_{1/2}(^{232}\text{Pa}) = 1.312 \pm 0.019$ days, $T_{1/2}(^{230}\text{Pa}) = 17.55 \pm 0.21$ days, $T_{1/2}(^{238}\text{Np}) = 2.24 \pm 0.22$ days, $T_{1/2}(^{236m}\text{Np}) = 22.27 \pm 0.65$ h, and $T_{1/2}(^{237}\text{U}) = 6.78 \pm 0.03$ days, all in agreement with recommended values (cf. Table I).

The yield Y of a reaction is defined as the number of the nuclei of a given radioisotope formed in the target per second of its irradiation. It was determined by the following formula:

$$Y = \frac{S(t_R/t_L)\lambda}{I_\gamma \varepsilon_\gamma (1 - e^{-\lambda t_e}) e^{-\lambda t_c} (1 - e^{-\lambda t_R})}, \tag{6}$$

where S is the area of the total absorption photopeak for the γ line of a given radioisotope, ε_γ is the efficiency of γ-quantum registration, I_γ is the relative gamma intensity, λ is the decay constant of the given radioisotope, t_e is the irradiation time, t_c is the time between the end of irradiation and the start of measurements (cooling time), and t_R and t_L are the real and live time of γ-ray spectroscopic measurement. The yield Y is related to the cross section σ of the reaction as

$$Y = I_p \nu_t \sigma, \tag{7}$$

TABLE I. Decay parameters of the daughter nuclei of reactions (1)–(5) taken from Ref. [22].

Product nucleus	Half-life $T_{1/2}$ (day)	γ energy E_γ (keV)	Relative γ intensity per decay I_γ (%)	γ detection efficiency, ε_γ (%)
^{232}Pa	1.31	894.35	19.6	0.162
^{230}Pa	17.4	951.88	29.6	0.153
^{238}Np	2.099	1028.53	18.23	0.144
^{236m}Np	0.937	94.65	10.5	0.704
		98.43	17.0	0.720
^{237}U	6.75	97.07	15.4	0.714
		101.06	24.5	0.729
		208.01	21.2	0.618

where ν_t is the number of target nuclei per unit area. The averages over multiple measurement values of Y and its statistical error were used when extracting the cross section from Eqs. (6) and (7). The obtained cross sections for reactions (1)–(5) are tabulated in Tables II and III. The quoted errors comprise, in addition to the statistical error, the systematic error (about 7%) contributed mainly by 5% uncertainty in ε_γ and 4.2% uncertainty in the cross section of the monitor reaction [21]. Our data are compared to the results of other experiments in Figs. 1 –5, from which the following observations can be done.

Our data on reaction (1) are comparable and in general agree with the previous measurements shown in Fig. 1, but somewhat overestimate the lowest energy data of Kmak (inverse triangles at $E_p < 15$ MeV) [6] and Kudo (full circles at $E_p < 13$ MeV) [4].

Our data on reaction (2) are comparable to the common trends of the data available from previous measurement as shown in Fig. 2. Note that the daughter nucleus ^{230}Pa of reaction (2) is a precursor of ^{230}U whose α-decay series may be of import to medical applications in the targeted α therapy for cancer (see, e.g., Refs. [7,9]). Table II shows that the cross section of the $(p, 3n)$ reaction increases steeply as a function of proton energy. The increase is steeper than for the (p, n) reaction data. At our highest energy $E_p = 17.0$ MeV, the ratio σ_{3n}/σ_n reaches about 5.6.

Figure 3 shows that the existing data for reaction (3) varies significantly (up to a factor of ∼2) between different publications. Our results are comparable to those of Guzhovskii (black triangles) [12], but contradict those of Aaltonen (open triangles) [11] and Ageev (black circles) [13].

Figure 4 shows that there are large discrepancies (up to a factor of ∼3) in the available data on reaction (4). Our data are comparable to common trend of the energy dependence. As in the case of thorium, the ratio σ_{3n}/σ_n for the uranium target increases steeply with E_p and reaches about 5.4 at our highest energy $E_p = 17.0$ MeV (see Table III).

The E_p dependence of the reaction (5) cross section is presented in Table III and Fig. 5. Our data fill partly the gap on reaction (5) in the relatively low energy region of $E_p < 20$ MeV.

IV. COMPARISON WITH TALYS1.96 MODEL PREDICTIONS

The cross-section data plotted in Figs. 1–5 were compared to the predictions of the nuclear reaction simulation TALYS1.96 [23]. The calculations were performed for different options of the following five ingredients of the code: the photon strength function (PSF), the optical model potential (OMP), the fission barrier (FB), the nuclear level density (NLD), and the pre-equilibrium mechanism (PEM). About two hundred combinations of the PSF, OMP, FB, NLD, and PEM options were tested.

It can be noted that the calculations showed a rather minor sensitivity of the considered cross sections to the PSF options (less than 10% spread between different options in the energy range $E_p = 12-17$ MeV). The same can be said concerning the OMP options, with the exception of the Jeukenne-Lejeune-Mahoux (JLM) option (*option JLM OMP*, see Ref. [24] and references therein) whose predictions for

TABLE II. The E_p dependence of the cross section σ_n for the ^{232}Th$(p, n)^{232}$Pa reaction and the cross section σ_{3n} for the ^{232}Th$(p, 3n)^{230}$Pa reaction.

Thorium subtarget	E_p (MeV)	σ_n (mb)	σ_{3n} (mb)
1	16.4 ± 0.08	17.54 ± 1.53	98.7 ± 6.0
2	15.3 ± 0.12	16.74 ± 1.48	22.2 ± 1.4
3	14.1 ± 0.13	14.92 ± 1.48	1.57 ± 0.15
4	12.9 ± 0.16	13.62 ± 1.45	
5	12.7 ± 0.18	13.22 ± 1.56	

TABLE III. Single-neutron emission cross section (σ_n), three-neutron emission cross section (σ_{3n}), and np emission cross section (σ_{np}) as a function of energy for ^{238}U$(p, n)^{238}$Np, ^{238}U$(p, 3n)^{236m}$Np, and ^{238}U$(p, np)^{237}$U reactions, respectively.

Uranium subtarget	E_p (MeV)	σ_n (mb)	σ_{3n} (mb)	σ_{np} (mb)
1	17.0 ± 0.36	12.89 ± 1.11	69.22 ± 5.06	39.90 ± 2.94
2	15.8 ± 0.10	12.50 ± 0.93	27.17 ± 1.99	21.84 ± 1.61
3	14.7 ± 0.14	11.90 ± 0.87	8.99 ± 0.69	11.67 ± 1.36
4	13.5 ± 0.27	9.86 ± 0.87		5.36 ± 0.44
5	12.0 ± 0.21	7.44 ± 0.71		1.20 ± 0.19

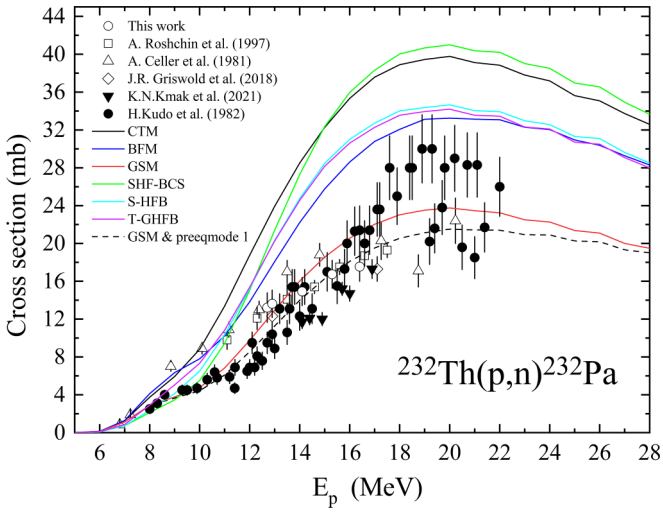

FIG. 1. The E_p dependence of the ^{232}Th$(p, n)^{232}$Pa reaction cross section.

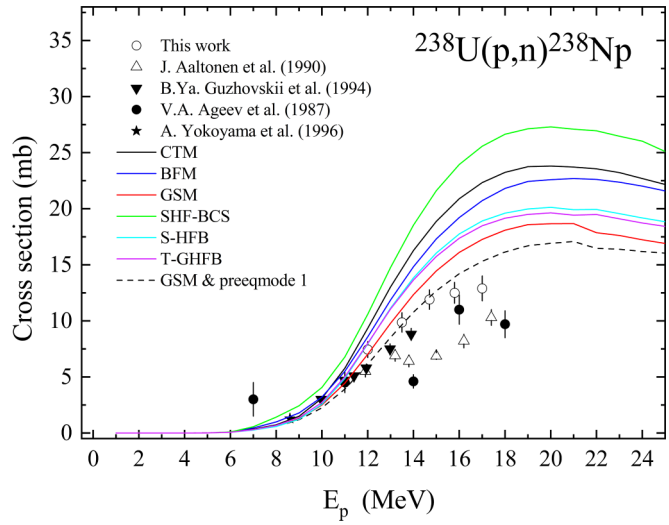

FIG. 3. The E_p dependence of the ^{238}U$(p, n)^{238}$Np reaction cross section.

$(p, 3n)$ reactions are almost fivefold lower compared to the cross sections with other OMP options. The tests have also shown that, with the JLM option, the predicted cross sections of $(p, 3n)$ reactions turn out to be strongly underestimated compared to the experimental data, irrespective of the choice of the PSF, FB, and NLD options. Hence, in the following evaluations, the default options of the PSF and OMP were chosen, namely, the simplified modified lorentzian (SMLO) option with the PSF tables suggested by Goriely and Plujko (see Ref. [23], the option *strength 9*) and the global optical model for the OMP proposed by Soukhovitskii *et al.* [25] for the description of experimental data concerning the nucleon scattering on actinide nuclei (the option *Soukho OMP*).

Further, the calculations showed a moderate sensitivity of the cross sections of (p, n) reactions to the FB options (about 35% spread between different options), while for the case of $(p, 3n)$ reactions the model predictions at various FB options differ by a factor of 5–10. A comparatively better description of the data on (p, n) reactions was achieved at the FB option *fismodel 5* (WKB approximation for the fission path model [26]). For the case of $(p, 3n)$ reactions only a very rough description of the data was provided at the default option *fismodel 1* ("experimental" fission barriers [27]). The other FB options were exhibiting larger discrepancies with the experimental data.

Further, all six options of the NLD (*ldmodel 1–ldmodel 6*) were tested in TALYS code (descriptions of the options are given in [23]), namely

ldmodel 1: Constant Temperature + Fermi gas model (CTM) [28],

ldmodel 2: Back-shifted Fermi gas Model (BFM) [28],

ldmodel 3: Generalised Superfluid Model (GSM) [29],

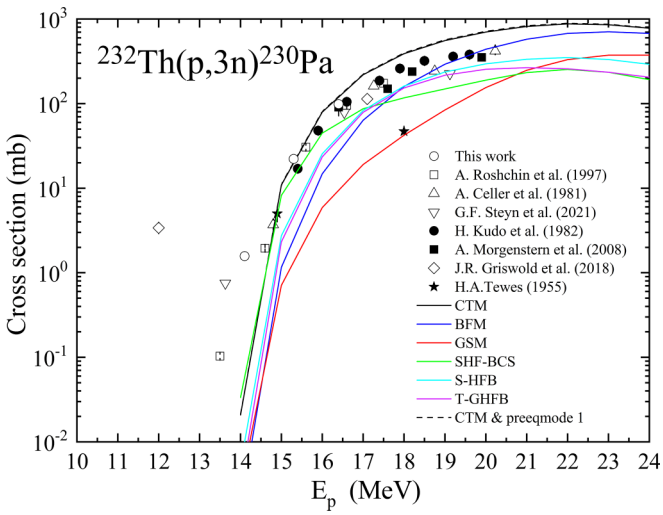

FIG. 2. The E_p dependence of the ^{232}Th$(p, 3n)^{230}$Pa reaction cross section.

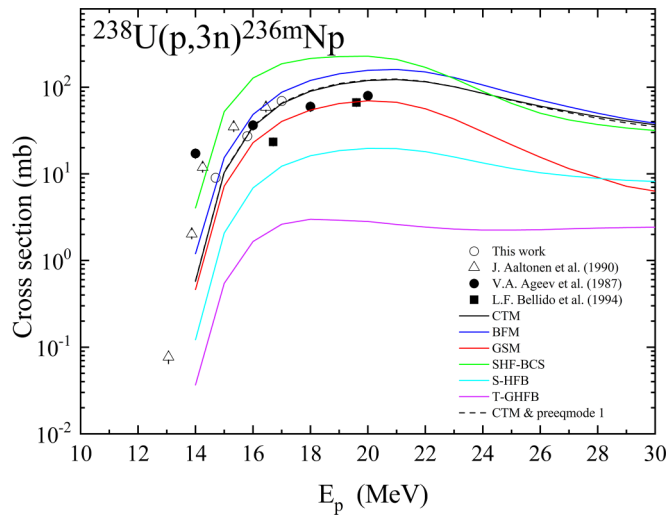

FIG. 4. The E_p dependence of the ^{238}U$(p, 3n)^{236m}$Np reaction cross section.

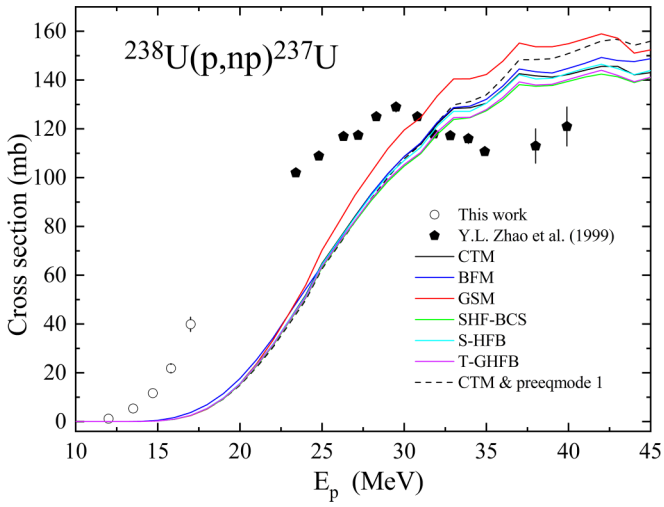

FIG. 5. The E_p dependence of the ^{238}U$(p, np)^{237}$U reaction cross section.

ldmodel 4: Skyrme-Hartree-Fock-BCS plus statistical model (SHF-BCS) [30],

ldmodel 5: Skyrme-Hartree-Fock-Bogolyubov plus combinatorial model (S-HFB) [31],

ldmodel 6: Temperature-dependent Gogny-Hartree-Fock-Bogolyubov level densities from Hilaire's combinatorial tables (T-GHFB) [32].

The NLD options were tested at chosen specified options of other ingredients, namely (see above)

(i) for the PSF - the option SMLO (the default option);
(ii) for the OMP - the option *Soukho OMP* (the default option);
(iii) for the FB - the option *fismodel 5* for one-neutron reactions (1) and (3), and the default option *fismodel 1* for multinucleon reactions (2), (4), and (5).

The predictions for the NLD options *ldmodel 1–ldmodel 6* concerning the cross sections of reactions (1)–(5) are plotted in Figs. 1–5 from which the following observations can be made:

(i) For the ^{232}Th$(p, n)^{232}$Pa reaction, the best (and almost satisfactory) description of the majority of the data at the energy range $E_p = 7-17$ MeV is achieved at the option GSM, as it is seen from Fig. 1.
(ii) For the ^{238}U$(p, n)^{238}$Np reaction, the best (although not satisfactory) description of the majority of the data at the energy range $E_p = 8-17$ MeV is achieved at the option GSM, as it is seen from Fig. 3.
(iii) For the ^{232}Th$(p, 3n)^{230}$Pa reaction, the best (although not satisfactory) description of the majority of the data at the energy range $E_p = 14-18$ MeV is achieved at the option CTM, as it is seen from Fig. 2.
(iv) For the ^{238}U$(p, 3n)^{236m}$Np reaction, the best (and almost satisfactory) description of the majority of the data at the energy range $E_p = 14-17$ MeV is achieved at the options CTM and BFM, as it is seen from Fig. 4.
(v) None of the considered combinations of the PSF, OMP, FB, and NLD options can reproduce (even roughly) the data on the ^{238}U$(p, np)^{237}$U reaction, as it is seen from Fig. 5; the predicted cross sections strongly underestimate (especially at $E_p < 18$ MeV) the experimental cross sections.

Finally, an attempt was undertaken to clarify whether the aforementioned inconsistencies between the model predictions and experimental data could be reduced depending on the choice of the option of another ingredient of the model—the pre-equilibrium mechanism (PEM) of the reactions considered. As expected (see Ref. [23] and references therein), at our energies the PEM can have a sizable contribution (along with the dominant compound nucleus mechanism) to the reaction cross section. All results of the model calculations plotted by solid curves in Figs. 1–5 were done at the default option of the PEM, preeqmode 2 (exciton model: numerical transition rates with energy-dependent matrix element [33]). Our calculations with three other options incorporated into the code (preeqmode 1, preeqmode 3, preeqmode 4) showed some improvement of the data description only at the option preeqmode 1 (exciton model: analytical transition rates with energy-dependent matrix element [34]) and only regarding one-nucleon ^{232}Th$(p, n)^{232}$Pa and especially ^{238}U$(p, n)^{238}$Np reactions (see dashed lines in Figs. 1–5).

V. SUMMARY

The cross sections of several proton-induced reactions were measured: ^{232}Th$(p, n)^{232}$Pa, ^{232}Th$(p, 3n)^{230}$Pa, ^{238}U$(p, n)^{238}$Np, ^{238}U$(p, 3n)^{236m}$Np, and ^{238}U$(p, np)^{237}$U. The proton beam energy ranged 12–17 MeV. We used the stacked-foil technique and the induced activation method. γ-ray spectroscopy was used to measure the activities of the various produced radioisotopes. The spectroscopic measurements were carried out in a low background underground laboratory (the Avan salt mine near Yerevan). The results, including 21 extracted cross-section data, were compared with previous measurements to elucidate some of the existing discrepancies measured by others. Our data on the reaction ^{232}Th$(p, n)^{232}$Pa falls within the error bars of the majority of the previous measurement data, but somewhat overestimates the lowest energy data of Kudo *et al.* (full circles at $E_p < 13$ MeV) [4] and Kmak *et al.* (inverse triangles at $E_p < 15$ MeV) [6]. Our data on the ^{232}Th$(p, 3n)^{230}$Pa reaction are comparable to the common trends of the data of Roschin *et al.* [3], Celler *et al.* [5], Steyn *et al.* [8], Kudo *et al.* [4], and Morgenstern *et al.* [9], but the same cannot be said for the data of Tewes *et al.* [10] and Griswold *et al.* [7]. The existing data for the ^{238}U$(p, n)^{238}$Np reaction vary significantly (by up to a factor of 2) between different publications. Our results are comparatively close to those of Guzhovskii *et al.* [12], but obviously contradict those of Aaltonen *et al.* [11] and Ageev *et al.* [13]. For the reaction ^{238}U$(p, 3n)^{236m}$Np, our results are qualitatively comparable to the data of Aaltonen *et al.* [11] and Ageev *et al.* [13], but contradict those of Bellido *et al.* [15]. We provide data for the first time in the low-energy range ($E_p < 20$ MeV) for producing ^{237}U in the

reaction ^{238}U$(p, np)^{237}$U. The existing data on this reaction (by Zhao *et al.* [16]) cover the range $E_p > 20$MeV.

The cross-section data are compared to the predictions of the nuclear reaction simulation code TALYS1.96, using different combinations of options of several main ingredients of the code, such as the photon strength function (PSF), the optical model potential (OMP), the fission barrier (FB), the nuclear level density (NLD), and the pre-equilibrium mechanism (PEM). The following conclusions can be inferred from a comparison to the model predictions:

(i) The predicted cross sections exhibit rather minor sensitivity to the choice of the PSF and OMP options (except for the JLM option of the OMP).

(ii) The model calculations showed a moderate sensitivity of the cross sections of (p, n) reactions to the FB options (about 35% spread between different options), while for the case of $(p, 3n)$ reactions the model predictions at various FB options differed by a factor of 5–10. A better description of the data on (p, n) reactions was achieved at the FB option *fismodel 5* (WKB approximation for fission path model). For the case of $(p, 3n)$ reactions only a very rough description of the data was provided at the default option *fismodel 1* (experimental fission barriers), while other FB options exhibited larger discrepancies with the data.

(iii) The strongest sensitivity of the predicted cross sections was manifested with respect to the NLD options. A comparatively better description of the data is achieved at the option GSM for ^{232}Th$(p, n)^{232}$Pa and ^{238}U$(p, n)^{238}$Np reactions, at the option CTM for the reaction ^{232}Th$(p, 3n)^{230}$Pa, and at the options CTM and BFM for the reaction ^{238}U$(p, 3n)^{236m}$Np.

(iv) A certain improvement of the data description for one-nucleon ^{232}Th$(p, n)^{232}$Pa reaction and especially ^{238}U$(p, n)^{238}$Np reaction can be achieved at the option *preeqmode 1* of the PEM.

(v) None of the considered combinations of the PSF, OMP, FB, NLD, and PEM options can reproduce (even roughly) the data on the reaction ^{238}U$(p, np)^{237}$U. The predicted cross sections strongly underestimate (especially at $E_p < 18$ MeV) the experimental cross sections.

ACKNOWLEDGMENTS

The authors express gratitude to the personnel of the C-18 cyclotron for providing the proton beam to irradiate an experimental installation and Prof. A. Aprahamian for valuable comments. The work was carried out with the financial support from the Higher Education and Science Committee of the Republic of Armenia within the framework of Scientific Project No. 21SCG-1C018.

[1] M. Arnould and S. Goriely, Prog. Part. Nucl. Phys. **112**, 103766 (2020).
[2] A. C. Cummings, E. C. Stone, B. C. Heikkila, N. Lal, W. R. Webber, G. Jóhannesson, I. V. Moskalenko, E. Orlando, and T. A. Porter, Astrophys. J. **831**, 18 (2016).
[3] A. Roshchin, S. Yavshits, V. Jakovlev, E. Karttunen, J. Aaltonen, and S. Heselius, Phys. At. Nucl. **60**, 1941 (1997).
[4] H. Kudo, H. Muramatsu, H. Nakahara, K. Miyano, and I. Kohno, Phys. Rev. C **25**, 3011 (1982).
[5] A. Celler, M. Luontama, J. Kantele, and J. Zylicz, Phys. Scr. **24**, 930 (1981).
[6] K. N. Kmak, D. A. Shaughnessy, and J. Vujic, Phys. Rev. C **103**, 034610 (2021).
[7] J. R. Griswold, C. U. Jost, D. W. Stracener, S. H. Bruffey, D. Denton, M. Garland, L. Heilbronn, and S. Mirzadeh, Phys. Rev. C **98**, 044607 (2018).
[8] G. F. Steyn, M. A. Motetshwane, F. Szelecsényi, and J. W. Brümmer, Appl. Radiat. Isot. **168**, 109514 (2021).
[9] A. Morgenstern, C. Apostolidis, F. Bruchertseifer, R. Capote, T. Gouder, F. Simonelli, M. Sin, and K. Abbas, Appl. Radiat. Isot. **66**, 1275 (2008).
[10] H. A. Tewes, Phys. Rev. **98**, 25 (1955).
[11] J. Aaltonen *et al.*, Phys. Rev. C **41**, 513 (1990).
[12] B. Ya. Guzhovskii, S. N. Abramovich, A. G. Zvenigorodskii, V. S. Rudnev, and S. V. Trusillo, Conf. Nucl. Data Sci. Technol. **1**, 390 (1994).
[13] V. A. Ageev *et al.*, Sov. J. Nucl. Phys. **46**, 392 (1987).
[14] A. Yokoyama *et al.*, Z. Phys. A **356**, 55 (1996).
[15] L. F. Bellido, V. J. Robinson, and H. E. Sims, Radiochem. Acta **64**, 11 (1994).
[16] Y. L. Zhao *et al.*, Radiochem. Acta **86**, 79 (1999).
[17] Nirta® Target Technology. Available online: https://www.iba-radiopharmasolutions.com/cyclotrons-equipment/.
[18] J. F. Ziegler, J. P. Biersack, and U. Littmark, *The Stopping and Range of Ions in Solids* (Pergamon, New York, 1985).
[19] A. A. Vasenko, I. V. Kirpichnikov, V. A. Kuznetsov, A. S. Starostin, A. G. Djanyan, V. S. Pogosov, S. P. Shachysisyan, and A. G. Tamanyan, Mod. Phys. Lett. A **5**, 1299 (1990).
[20] A. S. Hakobyan, A. Y. Aleksanyan, S. M. Amirkhanyan, H. R. Gulkanyan, T. V. Kotanjyan, V. S. Pogosov, and L. A. Poghosyan, J. Contemp. Phys. **55**, 111 (2020).
[21] https://www-nds.iaea.org/medical/monitor_reactions.html.
[22] USA National Nuclear Data Center database "Chart of Nuclides. Basic properties of atomic nuclei," https://www.nndc.bnl.gov/nudat3/.
[23] A. Koning, S. Hilaire, and S. Goriely, Eur. Phys. J. A **59**, 131 (2023).
[24] J. P. Jeukenne, A. Lejeune, and C. Mahaux, Phys. Rev. C **16**, 80 (1977).
[25] E. Sh. Soukhovitskii, S. Chiba, J.-Y. Lee, O. Iwamoto, and T. Fukahori, J. Phys. G: Nucl. Part. Phys. **30**, 905 (2004).
[26] M. Sin, R. Capote, and A. Ventura, Phys. Rev. C **74**, 014608 (2006).
[27] R. Capote *et al.*, Nucl. Data Sheets **110**, 3107 (2009).
[28] A. J. Koning, S. Hilaire, and S. Goriely, Nucl. Phys. A **810**, 13 (2008).

[29] A. V. Ignatyuk, J. L. Weil, S. Raman, and S. Kahane, Phys. Rev. C **47**, 1504 (1993).
[30] P. Demetriou and S. Goriely, Nucl. Phys. A **695**, 95 (2001).
[31] S. Goriely, S. Hilaire, and A. J. Koning, Phys. Rev. C **78**, 064307 (2008).
[32] S. Hilaire, M. Girod, S. Goriely, and A. J. Koning, Phys. Rev. C **86**, 064317 (2012).
[33] A. J. Koning and M. C. Duijvestijn, Nucl. Phys. A **744**, 15 (2004).
[34] C. Kalbach, Phys. Rev. C **33**, 818 (1986).